

Environmental Science Processes & Impacts

Accepted Manuscript



This is an *Accepted Manuscript*, which has been through the Royal Society of Chemistry peer review process and has been accepted for publication.

Accepted Manuscripts are published online shortly after acceptance, before technical editing, formatting and proof reading. Using this free service, authors can make their results available to the community, in citable form, before we publish the edited article. We will replace this *Accepted Manuscript* with the edited and formatted *Advance Article* as soon as it is available.

You can find more information about *Accepted Manuscripts* in the [Information for Authors](#).

Please note that technical editing may introduce minor changes to the text and/or graphics, which may alter content. The journal's standard [Terms & Conditions](#) and the [Ethical guidelines](#) still apply. In no event shall the Royal Society of Chemistry be held responsible for any errors or omissions in this *Accepted Manuscript* or any consequences arising from the use of any information it contains.

Insights into the complete and partial photooxidation of black carbon in surface waters [†]

Collin P. Ward^a, Rachel L. Sleighter^b, Patrick G. Hatcher^b, Rose M. Cory^{a}*

^aDepartment of Earth and Environmental Sciences, 2534 C.C. Little Building, 1100 North University Avenue, University of Michigan, Ann Arbor, Michigan 48109, USA

^bDepartment of Chemistry and Biochemistry, Physical Sciences Building, Room 3100, Old Dominion University, 4402 Elkhorn Avenue, Norfolk, Virginia 23529, USA

* Corresponding author: Phone: +1 734 615 3199; fax: +1 734-763-4690; email: rmcory@umich.edu

[†]Electronic Supplementary Information (ESI) available: See DOI: 10.1039/b000000x/

Environmental Impact

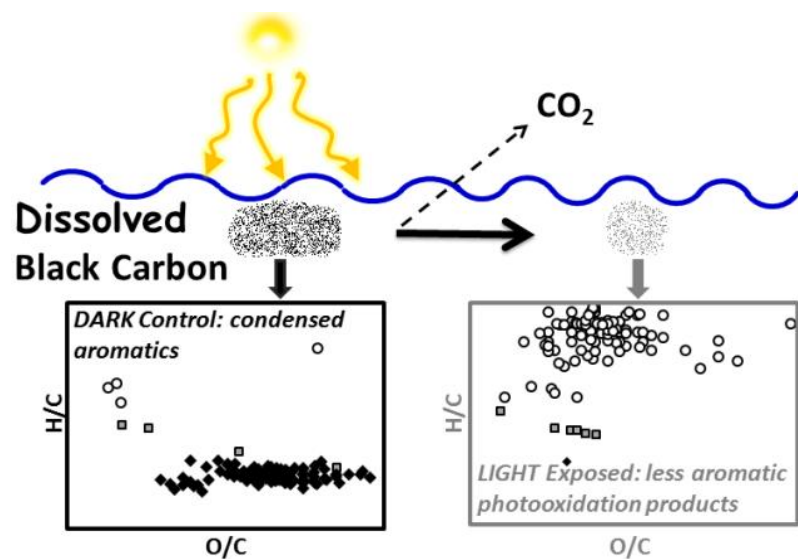
Black carbon is considered one of most recalcitrant components of organic carbon in the environment. The results of this study showed that dissolved black carbon was more susceptible to photooxidation compared to particulate black carbon. Partial photooxidation was the primary degradation pathway of dissolved black carbon, while a smaller fraction of dissolved black carbon was completely photooxidized to CO₂. These findings add further support to the role of sunlight as a sink for black carbon in surface waters; however, to refine the geochemical interpretation of this sink, work is needed to determine the reactivity of partially oxidized photoproducts of black carbon in the aquatic organic carbon pool.

Table of contents

Text:

Dissolved black carbon is more susceptible to photooxidation than particulate black carbon, and partial photooxidation of dissolved black carbon is a more important degradation pathway than complete photooxidation.

Graphic:



Abstract

Increasing wildfire activity in the Alaskan Arctic may result in new sources of black carbon (BC) to arctic watersheds. Black carbon, primarily comprised of condensed aromatics, is one of the most chemically recalcitrant fractions of organic carbon. However, lateral transfer of particulate and dissolved BC from soils to sunlit surface waters is increasingly suggested to result in the photochemical mineralization of BC to CO₂. While sunlight can also partially photooxidize aromatic compounds in surface waters, producing compounds with a higher O/C than the parent compound, this degradation pathway has not yet been identified for either particulate or dissolved BC. To address knowledge gaps on the photochemical degradation of particulate and dissolved BC, we quantified the complete and partial photooxidation of particulate and dissolved BC derived from arctic biomass as photochemical CO₂ production and O₂ consumption relative to dark controls. Concurrently, we investigated shifts in the chemical composition of dissolved BC following exposure to sunlight using UV-visible absorbance, fluorescence spectroscopy, and Fourier transform ion cyclotron resonance mass spectrometry (FT-ICR MS). The chemical and physical properties of BC produced from charring arctic biomass were similar to BC produced by wildfires in terrestrial ecosystems based on elemental analysis and FT-ICR MS. Based on the concentration of light-absorbing carbon in each fraction, dissolved BC was disproportionately more susceptible to complete and partial photooxidation compared to particulate BC. Upon exposure to sunlight, the predominant fate of dissolved BC was partial photooxidation, while a smaller fraction of dissolved BC was photomineralized to CO₂. Shifts in both the optical and mass spectrometry spectra suggested that condensed aromatics likely comprised the fraction of dissolved BC that was completely and partially photooxidized. To further refine the meaning of

sunlight as a sink for aquatic BC, the reactivity of partially oxidized photoproducts of BC in the aquatic organic carbon pool must be determined.

1. Introduction

Wildfire regime models predict that by the end of the 21st century, 62% of mid- to high-latitude regions will experience increases in wildfire activity.¹ These estimates include the Alaskan Arctic, a biome that has historically lacked wildfire activity over the last 10,000 years,² and is shifting to a fire regime of increased frequency and magnitude.^{3,4} Increased fire activity likely results in increased production of black carbon (BC), a molecularly diverse organic residue of wildfires formed from the incomplete combustion of organic matter. Black carbon has a longer residence time in soils compared to uncharred (parent) biomass⁵⁻⁷ and thus is one of the most recalcitrant components of the natural organic matter (NOM) pool, resulting in a long-term sink of atmospheric CO₂.^{6,7} While wildfires and associated sources of BC are widespread in the pan-arctic region,⁸ new sources of BC due to increased wildfire activity in the Alaskan Arctic may stabilize a fraction of the NOM pool in this critical region that stores vast amounts of C and is sensitive to climate change impacts on C storage.⁹⁻¹¹

The recalcitrant nature of BC is due to its chemical and physical properties, which vary along a continuum of carbon rich combustion residues from slightly charred biomass to soot.^{12,13} As charring temperature increases, atomic H/C and O/C ratios of the biomass decrease and the fraction of condensed aromatics in BC increases due to dehydration and condensation reactions.^{14,15} In contrast, the fraction of aliphatic compounds decreases with increasing charring temperatures. Thus, while BC is a mixture of compounds, its defining feature is hydrogen deficient condensed aromatic ring structures that are formed at high temperatures.¹⁶

For instance, approximately 65% of formulas detected in the Fourier transform ion cyclotron resonance mass spectrum (FT-ICR MS) of the water soluble fraction of 100-year-old fire-derived soil BC particles were classified as condensed aromatics formed from the

incomplete combustion of terrestrial biomass, while the remaining 35% were primarily thermally resistant aliphatics, e.g., compounds not derived from charred biomass.^{17,18} A similar distribution of compound classes was observed in a laboratory study comparing uncharred to charred oak.¹⁵ Of the condensed aromatic formulas detected in soil BC by FT-ICR MS, many are extensively substituted with oxygen-containing functional groups, which has been inferred to mean that oxidation and dissolution of BC occurs on centennial timescales.¹⁷⁻¹⁹

Abiotic and microbial oxidation and subsequent dissolution of condensed aromatics within soils results in the export of “water-soluble” BC from soils to sunlit surface waters,²⁰ where BC comprises a significant fraction (2 - 10%) of the riverine or marine dissolved organic matter (DOM) pool.^{21,22} Particulate BC may also be flushed from soils to surface waters, and thus mobilization and lateral transfer of particulate and dissolved BC from terrestrial ecosystems to rivers or oceans is an important loss process for wildfire produced BC in soils.^{8,17,18,21,23-26} Once in sunlit surface waters, sunlight may degrade the light-absorbing condensed aromatics found in both the particulate and dissolved BC given that photochemical reactions are a well-characterized sink for aromatics within the aquatic particulate organic matter and DOM pools.^{27,28} While no study has determined the susceptibility of particulate BC to degradation by sunlight, several studies have demonstrated that condensed aromatics associated with BC and detected in the riverine or marine DOM pools are susceptible to photochemical degradation.²⁸⁻³⁰ All condensed aromatics detected in Congo River DOM were absent from the mass spectrum after the sample was exposed to 57 days of simulated sunlight, suggesting that condensed aromatics were more susceptible to photodegradation than other types of compounds within the DOM pool.²⁸ In a subsequent study of BC in the marine DOM pool, Stubbins et al. (2012) reported that sunlight was the primary sink for dissolved BC resulting in the production of CO₂,

and estimated a half-life of < 800 years for photo-labile BC in the marine DOM pool, more than an order of magnitude shorter than the average apparent age of dissolved BC in the ocean.³⁰

These previous investigations of photochemical degradation of dissolved BC have demonstrated the loss of condensed aromatics in surface waters using FT-ICR MS²⁸ or detection as benzene polycarboxylic acids (BPCAs),^{29,30} which are molecular markers for condensed aromatics.³¹ Loss of condensed aromatics or BPCA markers upon exposure to sunlight has been interpreted as the complete photochemical oxidation of these compounds to CO₂. However, in addition to complete oxidation to CO₂, sunlight can partially oxidize dissolved aromatics,^{32–37} producing lower molecular weight products with higher O/C ratios than the parent compound. Thus, while studies have demonstrated the partial oxidation of aromatic compounds within bulk DOM³² or the decrease in condensation of BPCAs following exposure to sunlight,²⁹ no study has determined the degree to which photodegradation of condensed aromatics associated with aquatic BC results in complete oxidation to CO₂ vs. partial oxidation to compounds no longer detected as “BC.” Determining the degree of complete vs. partial oxidation of BC is important because CO₂ may once again participate in the carbon cycle, while the residence time and reactivity of partially oxidized photoproducts of BC that remain sequestered in the aquatic organic C pool is unknown. The disadvantage of using FT-ICR MS and BPCA markers to investigate the photochemical degradation of BC in riverine or marine waters is that there is no way to untangle the relative importance of complete or partial photooxidation of BC, given the presence of thousands of other dissolved organic compounds also undergoing photochemical degradation.

To address these knowledge gaps in the photochemical degradation of particulate and dissolved BC in surface waters, we investigated their susceptibility to complete and partial

photooxidation under conditions that allowed for the relative importance of each pathway to be estimated. Aqueous suspensions of particulate BC and aqueous solutions of dissolved BC derived from arctic biomass were exposed to sunlight, and the complete and partial oxidation was quantified as photochemical CO₂ production and photochemical O₂ consumption relative to dark controls. In order to connect degradation pathways of condensed aromatics associated with dissolved BC to complete or partial photooxidation, concurrent changes in the chemical composition of dissolved BC following exposure to sunlight were measured by UV-visible absorbance, fluorescence spectroscopy, and FT-ICR MS.

2. Methods

2.1 Production and elemental composition of precursor and charred biomass

Charred biomass was generated from a mixture of two precursor plant species following the guidelines of Hammes et al. (2006). Tealeaf willow (*Salix pulchra*) and feather moss (*Pleurozium schreberi*) were collected near Toolik Lake Field Station (68.63 N, 149.60 W), separated into subsamples, and placed into a Barnstead Thermolyne 6000 muffle furnace. The parent biomass was not dried before charring. The plant species were chosen because they are common in the Alaskan Arctic and were the major species charred in a recent tundra fire.⁴ To mimic the oxygen-free conditions that exist inside of charring biomass,³⁸ a stream of nitrogen gas was delivered to the furnace for 30 minutes prior to and throughout the duration of the charring. The average temperature throughout the five hour charring process, measured with a high-temperature ceramic thermocouple (Omega Engineering, Inc.), was 452 ± 2 °C ($n = 11$). Following charring, the samples were cooled overnight, ground with a mortar and pestle, and passed through a 425 μm sieve.

Elemental composition (C, H, and N) of pre-dried (65 °C for 24 hours) precursor and charred biomass was measured by Huffman Laboratories (Golden, CO). Ash content of the precursor and charred biomass was measured using loss-on-ignition following Hammes et al. (2006); however, a combustion temperature of 550 °C and a combustion time of 24 hours was used. Oxygen content of the precursor and charred biomass was estimated as the difference between the ash-free mass and the summed mass of the C, H, and N contents of the biomass. Sulfur content of the precursor and charred biomass was not measured. Thus, estimates of the mass of O may include mass due to small amounts of S (< 1%).³⁹ The charred biomass was used as the source of black carbon (BC) in this study.

2.2 Particulate and dissolved BC treatments

Two treatments were considered in this study: 1) unfiltered aqueous suspensions containing particulate and dissolved BC (pBC) and 2) filtered aqueous solutions containing dissolved BC (dBC). The pBC treatment was prepared by adding a known mass of BC to a known volume of laboratory-grade DI water, followed by equilibration with the atmosphere by stirring the suspension for 48 hours at room temperature in the dark. The C concentration of the pBC treatment was determined by multiplying the added mass of BC by the percent C of BC (determined by elemental analysis), dividing by the volume of DI water in suspension, and then converting to a molar basis. The dBC treatment was prepared by filtering the room temperature equilibrated pBC treatment (pre-combusted GF/F, ~ 0.7 µm, Whatman). The C concentration of the dBC treatment was quantified as CO₂ after high-temperature catalytic combustion using potassium hydrogen phthalate as the calibration standard, and likely was a minimum value due to

the presence of aromatic compounds less efficiently combusted to CO₂ when compared to the standard potassium hydrogen phthalate.⁴⁰

2.3 Light absorption of the pBC and dBC treatments

Absorption spectra of pBC were determined by subtracting the reflectance from the transmittance of the suspension using a 150 mm integrating sphere attached to a Cary 5000 UV-visible spectrophotometer (Varian, Inc.). This method corrects for the influence of light scattering on the absorption properties of suspended particles.⁴¹ The suspensions were stirred continuously during measurements to avoid settling and aggregation. Absorption spectra of a pBC dilution series made over the range of 3 to 30 mM-C resulted in a linear relationship ($r^2 = 0.99$, Fig. S1), suggesting similar contributions from scattering at all concentrations and multiple scattering effects were likely minimized at high concentrations. Absorption spectra of dBC were measured using a UV-visible spectrophotometer (Horiba Scientific). Decadic absorption coefficients of pBC and dBC were converted to Napierian absorption coefficients by multiplying by 2.303 and dividing by the pathlength of the 0.01 m quartz cuvette.

2.4 Photooxidation Experiments

2.4.1 Photochemical O₂ consumption and CO₂ production

The pBC and dBC treatments were pre-equilibrated with air in the dark at room temperature, transferred to acid and DI rinsed, pre-combusted, air-tight borosilicate vials (Labco Limited), and exposed to natural sunlight for 17 hours at Toolik Lake Field Station in June 2013. Dark controls were wrapped in aluminum foil. Average air temperature, measured every 5 minutes throughout the experiment, was 17 ± 2 °C (n = 209). Following the experiment, the light

exposed and dark control treatments were equilibrated to room temperature in the dark and analyzed for their dissolved oxygen concentration (O_2) using a membrane inlet mass spectrometer (MIMS; Bay Instruments) and dissolved inorganic carbon (DIC) concentration using a DIC analyzer (Apollo SciTech). In order to avoid clogging the inlets of the MIMS and DIC analyzer, particles in the pBC treatment were allowed to settle out of solution and the inlets were held directly above the settled particles during analysis. Photochemical O_2 consumption (μM) was quantified as the dark – light difference in O_2 concentration, while photochemical CO_2 production (μM) was quantified as the light – dark difference in DIC concentration.

Because several studies have reported the abiotic sorption of O_2 to pBC and desorption of CO_2 from pBC (e.g., Spokas and Reicosky 2009), rates of O_2 sorption and CO_2 desorption from the pBC produced in this study were measured to determine the influence of sorption or desorption on the photochemical O_2 consumption or CO_2 production. The same equilibrated pBC treatment as used in the photochemical experiments was transferred to acid and DI rinsed, pre-combusted, air-tight borosilicate vials. Dissolved oxygen and DIC concentrations were measured at the start and at the end of a two-week long incubation at room temperature in the dark. The measured rates of O_2 consumption and CO_2 production were 2.2 ± 0.1 and $0.8 \pm 0.2 \mu M \text{ day}^{-1}$ ($n = 3$), respectively. The rates were calculated as the amount of O_2 consumption or CO_2 production (μM) divided by the incubation time (days), assuming a constant rate throughout the incubation.⁴² Even though steps were taken to limit microbial activity (i.e., acid and DI rinsing, and pre-combustion of experimental vials), and no bacteria was added to the pBC treatment, the possibility of microbial activity cannot be ruled out. However, the rates of O_2 consumption or CO_2 production due to any combination of sorption, desorption, or microbial activity were approximately 10-fold lower than the rates of photochemical O_2 consumption and CO_2

production of 57.1 ± 4.5 and $8.6 \pm 1.6 \mu\text{M day}^{-1}$ ($n = 3$), respectively. Thus, at a minimum, photochemical processes accounted for 96% and 91% of O_2 consumption and CO_2 production in the pBC treatment, respectively. The contribution of sorption and desorption to photochemical O_2 consumption and CO_2 production was likely less important for the dBC treatment, which contained approximately 200-fold less C than the pBC treatment.

2.4.2 Effect of sunlight on dBC chemical characterization

A 4L dBC solution containing $< 40 \mu\text{M-C}$ was equally divided and transferred to two DI-rinsed UV-transparent whirlpak bags (Nasco). The light exposed dBC sample bag was placed in a Suntest XLS+ solar simulator for 48 hours (Atlas Material Testing, Inc.), while the dBC dark control bag was wrapped in aluminum foil and placed outside of the solar simulator. The Suntest XLS+ emits 3-fold more UV light (integrated from 305 to 395 nm) than June sunlight at Toolik Lake Field Station (Fig. S2). Thus, 48 hours of exposure in the solar simulator was equivalent to 6 days of exposure to natural sunlight at Toolik Lake Field Station. Within the experimental chamber of the solar simulator, the sample was placed in a temperature regulated pooling tray. The average temperature of the circulating water in the pooling tray, measured every ~ 5 hours using a Fisher Scientific Traceable thermocouple, was $16 \pm 1 \text{ }^\circ\text{C}$ ($n = 9$). Shifts in optical properties of dBC were similar when exposed to natural and simulated light sources, likely because there were little differences between the spectral shape and photon flux of natural and simulated light sources, and between the temperature throughout the field and lab experiments. Following the exposure to simulated sunlight, the light exposed and dark control dBC treatments were subjected to analysis by UV-visible absorbance spectroscopy, fluorescence spectroscopy, and mass spectrometry.

Collection of UV-visible absorption spectra was previously described (see section 2.3). Spectral slope ratio (S_R) was calculated from the absorption spectrum of each sample as the ratio of the slope from 275 to 295 nm to the slope from 350 to 400 nm following Helms et al. (2008). Fluorescence excitation-emission matrices (EEMs) of the samples were measured with an Aqualog fluorometer (Horiba Scientific). EEMs were collected over an excitation and emission range of 240 to 600 nm by excitation/emission increment pairs of 5/1.64 nm/nm, using an integration time of 4 s. EEMs were corrected for inner-filter and instrument specific excitation and emission effects in Matlab (version 7.12) using manufacturer provided excitation and emission correction spectra.⁴⁴ Blank EEMs were collected using fluorescent free, laboratory-grade DI water, and were subtracted from sample EEMs to minimize the influence of water Raman peaks. Finally, intensities of corrected sample EEMs were converted to Raman units.

The remaining ~ 1.6 L of the light exposed and dark control dBC treatments were reserved for Fourier transform ion cyclotron resonance mass spectrometry (FT-ICR MS). A maximum of 1.6 mmol-C of each dBC treatment was loaded onto the 1-g PPL solid-phase cartridges (Agilent Technologies) following Dittmar et al. (2008). Due to the qualitative nature of FT-ICR MS, C recovery from the PPL extraction was not quantified, although previous studies have reported up to 70% C recovery.⁴⁵ The PPL column was eluted with 100% LC-MS grade methanol, and diluted with LC-MS grade water to give a final sample composition of 50:50 (v/v) methanol:water. Samples were continuously injected into an Apollo II ESI ion source of a Bruker Daltonics 12 Tesla Apex Qe FT-ICR MS. Samples were injected at a rate of 120 $\mu\text{L h}^{-1}$ and were analyzed in negative ion mode. Ions were accumulated in a hexapole for 1.5 s before being transferred to the ICR cell, where 300 scans, collected with a 4 MWord time domain, were co-added for each sample. The summed free induction decay signal was zero-filled

once and Sine-Bell apodized prior to fast Fourier transformation and magnitude calculation using the Bruker Daltonics Data Analysis software. Similarly, a 50:50 (v/v) methanol:water blank spectrum was collected to test for contamination.

Mass spectra were externally calibrated using a polyethylene glycol standard and internally calibrated using fatty acids and other CH₂ homologous series naturally present in the sample.⁴⁶ Only peaks with a signal to noise ratio ≥ 4 were assigned molecular formulas. A molecular formula calculator (Molecular Formula Calc v.1.0 ©NHMFL, 1998) generated formulas using carbon, hydrogen, oxygen, nitrogen, and sulfur. Mass lists were screened to remove peaks also detected in the blank spectrum.²⁸ Only formulas that agreed within an error of $\leq \pm 0.5$ ppm to the calculated exact mass of the formula were considered, and all formulas were screened to meet the following criteria:²⁸

1) Double bond equivalents (DBE) ≥ 0 , and must be a whole number, where:

$$\text{DBE} = 1 + 0.5(2C - H + N) \quad (1)$$

- 2) $C \leq 50$
- 3) $2 \leq H \leq (2C + 2)$
- 4) $0 \leq O \leq (C + 2)$
- 5) $O/C < 1.2$
- 6) $0.3 \leq H/C \leq 2.25$
- 7) $N/C < 0.5$
- 8) $S/C < 0.2$

The modified aromaticity index (AI_{mod}), which reflects the C-C double-bond density of each formula, was calculated following equation 2:⁴⁸

$$AI_{\text{mod}} = (1 + C - 0.5O - S - 0.5H) / (C - 0.5O - S - N) \quad (2)$$

The formulas were categorized into three compound classes according to their AI_{mod} : aliphatic ($AI_{\text{mod}} < 0.5$), aromatic (non-condensed; $0.67 < AI_{\text{mod}} \leq 0.5$), and condensed aromatic ($AI_{\text{mod}} \geq 0.67$). Although the trends were similar for number and abundance-weighted data, number-weighted averages of molecular weight, atomic ratios, and indices were used to characterize dBC because the dark control and light exposed dBC treatments exhibited substantial differences in molecular composition (i.e., compound class distribution). Using differences in number-weighted averages, rather than abundance-weighted averages, has been recommended for aquatic DOM that exhibits large differences in molecular composition.⁴⁹

3. Results

3.1 Elemental composition of precursor and charred biomass

Charring altered the elemental composition of the arctic biomass. The charred biomass had significantly higher %C and lower %O and %H compared to the precursor biomass (Table 1). It follows that charring decreased the atomic H/C ratio from 1.45 to 0.40 and the atomic O/C ratio from 0.53 to 0.09 (Table 1). The elemental composition of the charred biomass was similar to the charcoal and soot classes of residues comprising the black carbon (BC) combustion continuum.³⁸ Thus, aqueous suspensions and solutions of the charred biomass were used to determine the light absorption and photooxidation of BC.

3.2 Filter separation of pBC and dBC treatments

Equilibration of BC in laboratory-grade DI water for 48 hours resulted in less than 1% of the initial C partitioning to the operationally defined dissolved phase, based on GF/F filtration. For example, BC suspensions prepared at C concentrations ranging from 15 to 118 mM-C

resulted in dissolved C concentrations ranging from 63 to 279 $\mu\text{M-C}$ after filtration (Fig. S3). Because > 99% of the C in the unfiltered treatment was retained by a GF/F filter, independent of the initial C concentration, the unfiltered treatment was operationally defined as particulate BC (pBC). Similarly, the filtered BC treatment was operationally defined as dissolved BC (dBC).

3.3 Light absorption and photooxidation of pBC vs. dBC

The absorption spectrum of pBC, containing 15 mM-C, decreased with increasing wavelength in the UV, with absorption coefficients ranging from $25.5 \pm 2.7 \text{ m}^{-1}$ at 280 nm to $22.6 \pm 2.1 \text{ m}^{-1}$ at 400 nm ($n = 2$; Fig. 1). The absorption coefficient remained relatively stable across the visible portion of the spectrum, e.g., the absorption coefficient at 600 nm was 94% of the absorption coefficient at 400 nm. The pBC treatment consumed $40 \pm 3 \mu\text{M-O}_2$ upon exposure to sunlight relative to the dark control ($n = 3$; Fig. 2). For the same suspension, photochemical CO_2 production was $6 \pm 1 \mu\text{M}$ ($n = 3$), seven-fold less than photochemical O_2 consumption (Fig. 2).

The absorption spectrum of dBC, containing $63 \pm 2 \mu\text{M-C}$, decayed exponentially across the UV and the visible, with absorption coefficients ranging from $4.9 \pm 0.4 \text{ m}^{-1}$ at 280 nm to $0.73 \pm 0.1 \text{ m}^{-1}$ at 600 nm ($n = 3$; Fig. 1). The dBC treatment consumed $42 \pm 6 \mu\text{M-O}_2$ and produced $7 \pm 1 \mu\text{M-CO}_2$ upon exposure to sunlight relative to the dark control ($n = 3$; Fig. 2). Photochemical CO_2 production was six-fold less than photochemical O_2 consumption (Fig. 2).

Despite 200 times greater C concentration and a six-fold higher absorption coefficient (at 305 nm) between the pBC and dBC treatments, there was no detectable difference in the photochemical O_2 consumption or the photochemical CO_2 production between these treatments (not significantly different by unpaired Student's t-test, $p = 0.3$; Fig. 2). This result suggested

that the majority of the O₂ consumed and CO₂ produced upon exposure to sunlight was associated with the photooxidation of dBC instead of pBC. Thus, only dBC was subjected to mass balance analysis and chemical characterization following exposure to sunlight.

The concentration of C in the dBC treatment ranged from a measured minimum of 61 μM-C to an estimated maximum of 77 μM-C (Fig. 3, Table S1), 20% higher than the maximum measured concentration because aromatic compounds have been shown to be on average 20% less efficiently oxidized to CO₂ by high-temperature catalytic combustion compared to aliphatic compounds used as standards for quantifying C.⁴⁰ Based on the range of C estimated in the dBC treatment and given that the photochemical production from the dBC treatment was 6 - 8 μM CO₂, 8 - 13% of the C in the dBC was mineralized to CO₂ by sunlight (Fig. 2, Table S1). Assuming that 1 mol of O₂ was consumed for 1 mol of CO₂ produced, the difference between photochemical O₂ consumption and CO₂ production (29 - 39 μM-O₂; Fig. 2, Table S1) was the range of O₂ incorporated into organic compounds within the dBC treatment. We converted this O₂ uptake concentration to carbon units representing the concentration of partially oxidized C formed by oxygen incorporation to dBC compounds using the following two assumptions. First, we assumed that the partially oxidized photoproducts would have O/C stoichiometry within the range observed from the mass spectrum of the dark dBC treatment (0.05 - 1.1; consistent with the average value reported for bulk DOM).⁵⁰ Second, we took a mass balance approach to constrain the upper limit of partially oxidized C that could be produced. The maximum amount of C that could be partially oxidized was the maximum estimate of C initially present in the dBC treatment (77 μM-C) minus the amount of C in dBC that was mineralized to CO₂ (6 - 8 μM-C, Fig. 2). Using these assumptions, we estimated that at the highest O/C ratio detected in the dBC dark control (1.1 mol O per mol C) 29 - 39 μM-O₂ incorporation yields 52 - 72 μM partially

oxidized C, meaning 70 - 117% of the maximum amount of C in the dBC treatment was partially oxidized by sunlight (Fig. 3, Table S1). The lowest O/C ratio detected in the dBC dark control that did not produce more oxidized C than was available for oxidation in the dBC treatment was 0.82 mol O per mol C; using this ratio with the minimum measured O₂ incorporation of 29 μM-O₂ yielded 70 μM of partially oxidized C. Thus, the best estimate was that 52 - 70 μM-C or 68 - 91% of the C in the dBC treatment was partially oxidized by sunlight (Fig. 3, Table S1).

3.4 Effects of sunlight on the chemical characterization of dBC

The fluorescence spectrum of dBC was comprised of two peaks characterized by excitation/emission wavelength maxima at 245/415 nm/nm (peak 1) and 305/415 nm/nm (peak 2) (Fig. 4, Table S2). Compared to the dBC dark control, fluorescence intensities of peak 1 and peak 2 decreased by $81 \pm 3\%$ and $88 \pm 1\%$, respectively (Fig. 4, Table S2). In addition to a loss in fluorescence intensity, there was a decrease in absorption coefficients and a shift in the spectral slope ratio (S_R) compared to the dark control. Absorption coefficients of dBC decreased by $24 \pm 1\%$ (at 305 nm) compared to the dark control (Table S2). Because the loss of absorption following exposure to sunlight was greater at longer wavelengths compared to shorter wavelengths, there was an $18 \pm 9\%$ increase in the spectral slope ratio, a proxy that has been used to evaluate shifts in average molecular weight of aquatic dissolved organic carbon upon exposure to sunlight (Table S2).⁴³

Over 2000 molecular formulas were assigned to the peaks detected in the mass spectrum of the dBC dark control (excluding contributions from ¹³C isotopes, Table 2). The mass spectral peaks spanned a mass range of 250-700 Da, with an average molecular weight of 434 Da (Table 2). The average H/C and O/C of all assigned formulas was 0.88 and 0.37, respectively (Table 2).

The average number of double bond equivalents (DBE) per formula, an indicator of the degree of condensation, was 14 (Table 2). The average modified aromaticity index (AI_{mod}) of each formula, a proxy for aromatic C content, was 0.54 (Table 2). On a number basis, the majority of formulas were classified as condensed aromatics (53%) or aliphatics (36%), while aromatics (non-condensed) comprised a minority fraction (11%; Table 2, Fig. 5). Analysis of the condensed aromatic, aromatic, and aliphatic formulas in van Krevelen space showed that within each compound class, there was a range of elemental composition (Fig. 5). Condensed aromatics were centered on an H/C of 0.50, spanning a range from 0.31 to 0.73. By definition, aromatic and aliphatic formulas had higher H/C ratios than condensed aromatics, but the aliphatics spanned a larger range of H/C than the aromatics and condensed aromatics (Fig. 5). While all three compound classes spanned a similar O/C range, the mean O/C of aliphatics and aromatics was lower when compared to condensed aromatics (Fig. 5).

Compared to the dBC dark control, the mass spectrum of the light exposed dBC treatment contained 42% fewer assigned formulas, and there was a shift in the average elemental composition and compound class distribution (Fig. 5). After sunlight exposure, there was a decrease in the average molecular weight, DBE, and O/C, while there was an increase in the average H/C (Table 2). Compared to the dark control, the number and abundance of condensed aromatics decreased by 43 and 51%, respectively, while the number and abundance of aliphatics increased by 49 and 55%, respectively (Table 2). Of the 100 most abundant formulas that were identified only in the dBC dark control (not in the light-exposed dBC treatment), 92 were condensed aromatics (Fig. 6), suggesting the compounds corresponding to these formulas were preferentially removed by photooxidation. In contrast, of the 100 most abundant formulas that were found only in the light exposed dBC treatment (e.g., not detected in the dBC dark control),

93 were aliphatics (Fig. 6), suggesting that the compounds corresponding to these formulas were preferentially produced upon exposure to sunlight. Thus, following exposure of dBC to sunlight, the majority of molecular formulas on a number basis was aliphatics (85%), with condensed aromatics (10%) and aromatics (5%) comprising smaller fractions (Fig. 5, Table 2).

In addition to a shift in the distribution of major compound classes within dBC, there was a shift in the elemental composition of the formulas in each compound class following sunlight exposure. Compared to the dBC dark control, the average H/C of aliphatics, aromatics, and condensed aromatics increased following light exposure (Table 2). Compared to the dBC dark control, sunlight exposure increased the average O/C of condensed aromatics, but decreased the average O/C of aromatics and aliphatics (Table 2). Additionally, following sunlight exposure, the range of O/C exhibited by aliphatic formulas in the dBC treatment increased, while the range of O/C exhibited by condensed aromatics and aromatics decreased (Fig. 5).

4. Discussion

4.1 Characterization of BC

The chemical and physical properties of the black carbon (BC) produced in this study were similar to BC produced by wildfires in terrestrial ecosystems. The atomic H/C and O/C ratios of the BC produced in this study were within the range reported for BC-rich residues that comprise the BC combustion continuum.³⁸ The weak exponential decay throughout the visible region of the absorption spectrum of particulate BC (pBC) was consistent with absorption spectra of particulate BC aerosols in the atmosphere also lacking strong wavelength dependence throughout the visible region.⁵¹ That only a trace fraction of pBC (< 1% of C in the pBC treatment) was operationally defined as water soluble by GF/F filtration was consistent with the

similarly low aqueous solubility of wildfire produced soil BC¹⁷ and laboratory produced BC.^{24,52,53} The lower H/C and O/C of the pBC treatment (determined using elemental analysis) compared to the H/C and O/C of the dissolved BC (dBC) treatment (determined using FT-ICR MS), suggested that less condensed, more oxidized compounds partitioned to the dissolved phase (Tables 1 and 2). Given that the elemental composition of dissolved organic matter (DOM) determined using elemental analysis and FT-ICR MS are in close agreement ($\pm 15\%$),⁵⁴ and the differences in elemental composition observed between the pBC and dBC treatments were $> 15\%$ (Tables 1 and 2), we interpreted these differences in elemental composition as significant. The observation of less condensed and more oxidized compounds in the dissolved phase was consistent with previous reports of the Fourier transform infrared absorption spectra of pBC and dBC, where dBC had more oxygen containing functional groups than pBC, suggesting that dBC had higher polarity and H-bonding with water than pBC.⁵⁵

The elemental composition of formulas assigned to peaks detected in the dBC dark control FT-ICR mass spectrum was similar to the elemental composition of formulas from the soluble fraction of wildfire-derived 100-year-old soil BC particles, suggesting that the chemical composition of dBC used to investigate photochemical reactivity in this study was similar to dBC exported from terrestrial to aquatic ecosystems.^{17,18} For example, the range of H/C and O/C exhibited by the formulas in the dBC dark control overlapped with the H/C and O/C range reported for compounds in the wildfire-derived dBC¹⁸ (0.1 - 2.0 and 0.0 - 0.7, respectively). Likewise, assignment of compound classes based on the modified aromaticity index (Eqn. 2) showed that condensed aromatics accounted for the majority (53%) of formulas assigned to the peaks in the mass spectrum of the dBC dark control, similar to the fraction of peaks assigned to condensed aromatics in wildfire-derived dBC (65%).¹⁷

Condensed aromatics, such as those detected in the mass spectrum of wildfire-derived dBC,¹⁷ have been attributed to the incomplete combustion of organic matter and thus are included in the operationally defined pool of BC. However, the thermal origin of the aliphatics increasingly detected alongside condensed aromatics in environmental and laboratory produced BC is less clear.^{15,17,38} Based on their elemental composition, Hockaday et al. (2006) classified the aliphatics detected in wildfire-derived dBC as “lignin-like” compounds and suggested that these aliphatics were derived from the thermally resistant, uncharred woody domains of BC. The majority of the aliphatics in the dBC dark control (~81%) overlapped in elemental composition with those detected by Hockaday et al. (2006) and thus could also be classified as thermally resistant “lignin-like” compounds. However, biomass can undergo partial combustion to yield thermally altered, “lignin-like” aliphatic compounds.^{15,55} Consequently, the aliphatics in the dBC dark control were likely a mixture of thermally resistant and partially combusted compounds.

4.2 Photochemical reactivity of dBC

Dissolved BC was disproportionately more photoreactive compared to the C in the pBC treatment (Fig. 2). The photochemical O₂ consumption and CO₂ production attributed to dBC, constrained by the mass balance estimates of C in the dBC treatment, indicated that 8-13% of the C in the dBC treatment was photomineralized to CO₂, while 68-91% of the C was partially photooxidized to compounds remaining in the dBC treatment (Fig. 3, Table S1). Beginning with photomineralization, we evaluated three possibilities for the class of compounds meeting this fate: (1) condensed aromatics and aromatics were photomineralized to CO₂, (2) aliphatics were photomineralized to CO₂, or (3) a mixture of compounds (condensed aromatics, aromatics, and aliphatics) was mineralized to CO₂. Evidence in support of preferential photomineralization of

condensed aromatics and aromatics was that 89% of condensed aromatics and 73% of aromatics were absent from the mass spectrum following sunlight exposure (Table 2). Furthermore, most of the formulas unique to the dBC dark control were condensed aromatics (Figs. 5 and 6), suggesting that these compounds were degraded upon exposure to sunlight and thus absent from the mass spectrum of light-exposed dBC. These results were consistent with a previous study showing loss of proxy compounds for condensed aromatics in the marine dBC pool following exposure to sunlight.²⁹ Consistent with the loss of condensed aromatics and aromatics following exposure to sunlight was the decrease in absorption coefficients by 24% and the decrease in fluorescence intensities by > 80% (Fig. 4, Table S2). Condensed aromatics and aromatics are chromophoric (i.e., light absorbing) and were thus much more likely to account for the light absorbing and emitting spectra of dBC compared to the non-light absorbing aliphatics.

Evidence against the preferential photomineralization of aliphatics was that aliphatics were the most abundant formulas unique to the light exposed dBC treatment (Figs. 5 and 6), suggesting that aliphatics were likely produced by the photochemical degradation of condensed aromatics and aromatics. While the simultaneous loss of condensed aromatics and aromatics and production of aliphatics is consistent with photochemical degradation studies of DOM,²⁸ the production of aliphatics upon exposure to sunlight was inconsistent with an expected loss if aliphatics were preferentially photomineralized to CO₂. Although it was possible that differences in extraction and ionization efficiency of compounds in the dBC treatment before and after exposure to sunlight masked some changes in compound distributions, shifts in the mass and optical spectra together following exposure to sunlight suggested that condensed aromatics (and non-condensed aromatics to a smaller degree) most likely comprised the fraction of dBC that was photomineralized to CO₂.

Evaluating the same three possibilities for the class of compounds that was partially photooxidized, we suggest that the most likely explanation was that condensed aromatics were preferentially partially oxidized by sunlight. There was a decrease in the average O/C of aromatics and aliphatics, while in contrast there was an increase in the average O/C of condensed aromatics remaining after photooxidation compared to the dark control, suggesting that condensed aromatics were more susceptible to partial photooxidation than aromatics and aliphatics (Table 2). The decrease in O/C for aromatics and aliphatics was likely due to the breakdown of higher molecular weight compounds leading to the production of less oxidized (lower O/C) and more oxidized (higher O/C) compounds compared to the parent compound. We hypothesize that the more oxidized photoproducts were of lower molecular weight^{34,37} and thus were likely outside the analytical window of detection using FT-ICR MS (250 - 700 m/z), consistent with the decrease in average molecular weight for the remaining aromatics and aliphatics (Table 2). The increase in O/C of the condensed aromatics after exposure to sunlight was consistent with the partial photooxidation of aromatics yielding photoproducts with higher O/C ratios than the parent compound.³²⁻³⁷ To account for the observed increase in O/C of 0.02 (for condensed aromatics, Table 2), approximately 504 condensed aromatics would have had to incorporate one oxygen (O) upon exposure to sunlight. The partial photooxidation of 504 condensed aromatics was equivalent to 24% of the 2058 formulas in the dBC dark control and thus less than the estimated 68-91% of C that was partially photooxidized based on mass balance calculations (Table 2, Fig. 3).

Possibilities for the “missing” partially oxidized C include: more than one O was incorporated into condensed aromatics, and partial photooxidation of condensed aromatics may have produced oxidized low molecular weight products that fell outside the analytical window of

detection using FT-ICR MS (250 - 700 m/z). Partial photooxidation of aquatic DOM produces oxidized, low molecular weight compounds^{34,37} outside the analytical window of detection using FT-ICR MS. Consistent with the production of low molecular weight photoproducts, condensed aromatics exhibited an 11% decrease in average molecular weight upon exposure to sunlight (Table 2). In addition, there was a shift in the spectral slope ratio (S_R) of the dBC absorption spectrum, indicating decreased average molecular weight of the light-absorbing fraction of dBC (i.e., condensed aromatics and aromatics) following sunlight exposure (Table S2). In contrast, aromatics and aliphatics exhibited a smaller decrease in average molecular weight upon exposure to sunlight compared to condensed aromatics (6% and 7%, respectively; Table 2). Thus, the production of low molecular weight photoproducts most likely resulted from the partial photooxidation of condensed aromatics compared to aromatics and aliphatics.

4.3 Environmental implications: photochemical fate of BC

The finding that the smaller operationally defined dBC treatment was disproportionately more susceptible to photooxidation than the larger pBC treatment strongly suggests that the size of BC compounds transferred from terrestrial to aquatic ecosystems may influence the susceptibility of BC to photooxidation. However, considering a larger size fraction of BC particles was used in the pBC treatment ($< \sim 425 \mu\text{m}$) than is expected to be transferred from terrestrial to aquatic ecosystems ($< 200 \mu\text{m}$),²⁴ and no study has quantified the size distribution of BC in arctic surface waters, the apparent resistance of pBC to complete and partial photooxidation under the experimental conditions tested here may not apply across the size fraction of BC particles in arctic surface waters.

The balance of evidence suggested that of the formulas present in the dBC treatment, condensed aromatics likely accounted for the majority of complete and partial photooxidation. Considering that most studies define, quantify, and study dBC based on a measurement of condensed aromatics in the bulk DOM pool,^{22,23,28,29} our findings on the photochemical fate of soluble condensed aromatics from charred biomass are relevant for the fate of water-soluble BC produced by fires and transferred from terrestrial to aquatic ecosystems. Furthermore, complete and partial photooxidation of dBC in this study occurred on timescales similar to residence times in sunlit surface waters and transit time in rivers (e.g., days to weeks).⁵⁶ Given that the minimum estimate of partially photooxidized C (68% of C in the dBC treatment) was five-fold higher than the maximum estimate of complete photooxidation to CO₂ (13%, Fig. 3), the predominant fate of dBC exposed to sunlight was partial photooxidation to less aromatic photoproducts with unknown susceptibility to further degradation.

Sunlight has previously been reported as the primary sink for marine dBC, with CO₂ reported as the main photoproduct.²⁹ For example, exposing DOM collected from the deep North Atlantic to six days of simulated sunlight resulted in a 29% decrease in the dBC fraction of the DOM. The dBC fraction of the DOM pool was quantified as benzene polycarboxylic acids (BPCAs), molecular markers for the combustion derived condensed aromatic fraction of DOM.³¹ However, presence, absence, or decreasing concentrations of the proxy BPCA markers does not distinguish between complete or partial photooxidation. While there are likely differences in the photoreactivity between freshly charred biomass and “aged” black carbon in the marine DOM pool, our findings suggest that the majority of the photodegraded dBC in the North Atlantic was not completely oxidized to CO₂ but was instead converted to partially oxidized C no longer recognizable as “black carbon” (e.g. not detectable as BPCAs). Because the susceptibility of

these partially oxidized photoproducts to further degradation is unknown, so is the long-term stability of these compounds in the DOM pool. Thus, to better refine the interpretation of sunlight as a sink for dBC, our results suggest that further work is required to relate the loss of condensed aromatics to their complete or partial photooxidation and to test the susceptibility of the partially oxidized photoproducts to further degradation.

The changing fire regime in the Alaskan Arctic will likely provide new sources of BC to arctic soils. Given that microbial degradation of BC is temperature sensitive,⁵⁷ the lower temperatures in arctic soils compared to temperate or tropical regions may limit microbial degradation, and in turn increase the relative importance of other BC degradation processes such as photooxidation. Thus, the persistence of BC in arctic soils may be controlled by the lateral transfer of BC from arctic soils to sunlit surface waters and the subsequent photooxidation of BC. Accordingly, the strong terrestrial-aquatic linkage in the Arctic associated with the annual flush of soil C to sunlit surface waters⁵⁸ may facilitate opportunities for the photochemical oxidation of BC during riverine transport to the Arctic Ocean.

Acknowledgements We thank M. Brennaman, J. Dobkowski, S. Fortin, K. Harrold, S. Michael, Y. Nguyen, and researchers, technicians, and support staff of the Toolik Lake Arctic LTER for assistance. Special thanks to G. W. Kling for his invaluable advice during the research planning stages. Thanks to the staff at College of Sciences Major Instrument Cluster (COSMIC) at Old Dominion University for assistance with FT-ICR MS analysis. We also thank the anonymous reviewers, whose comments significantly improved the quality of this manuscript. Research was supported by NSF OPP-102327.

Figure descriptions

Figure 1. Duplicate and triplicate absorption spectra of the pBC and dBC treatment containing 15 mM-C and 63 μ M-C, respectively. Values show Napierian absorption coefficients (m^{-1}).

Figure 2. Effect of sunlight on the dissolved O_2 and CO_2 concentrations (μ M) of the dark control and light exposed dBC and pBC treatments containing 63 μ M-C and 15 mM-C, respectively.

The series on the left is dark and light dissolved O_2 concentration, while the series on the right is dark and light dissolved CO_2 concentration. Dark controls were wrapped in aluminum foil. Error bars show \pm standard deviation from the mean ($n = 3$).

Figure 3. Mass balance analysis of the complete and partial photooxidation of C in the dBC treatment. The minimum estimate of partially photooxidized C (68%) was five-fold higher than the maximum estimate of complete photooxidation to CO_2 (13%), suggesting that the predominant fate of dBC exposed to sunlight was partial photooxidation.

Figure 4. Effect of sunlight on EEMs of the dark control (left spectrum) and light exposed (right spectrum) dBC treatments. The spectra are characterized by excitation/emission wavelength maxima at 245/415 nm/nm (peak 1) and 305/415 nm/nm (peak 2). Compared to the dBC dark control, the fluorescence intensities of peak 1 and peak 2 in the light exposed dBC treatment decreased by 81% and 88%, respectively.

Figure 5. Van Krevelen diagrams for formulas assigned via FT-ICR MS analysis of the dark control (A and B) and light exposed dBC treatment (C and D). The color scheme in (A) and (C) corresponds to the class of each formula based on AI_{mod} , while the color scheme in (B) and (D) corresponds to the relative abundance of each formula.

Figure 6. Van Krevelen diagram (A) shows the 100 most abundant formulas found only in the dBC dark control treatment. Van Krevelen diagram (B) shows the 100 most abundant formulas found only in the light exposed dBC treatment. Each diagram is colored according to the compound class of each formula, based on AI_{mod} .

Figure 1.

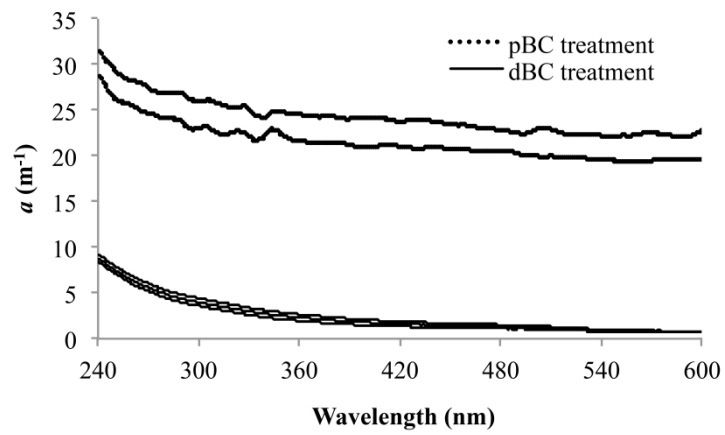


Figure 2.

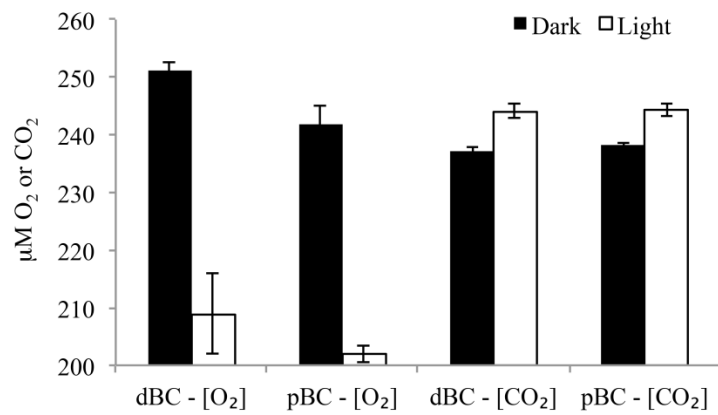


Figure 3.

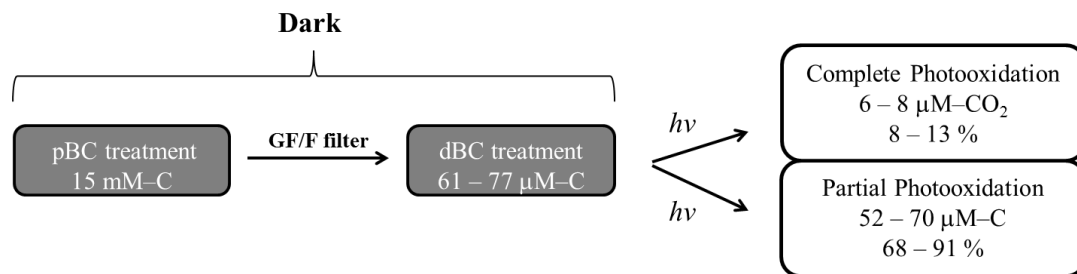


Figure 4.

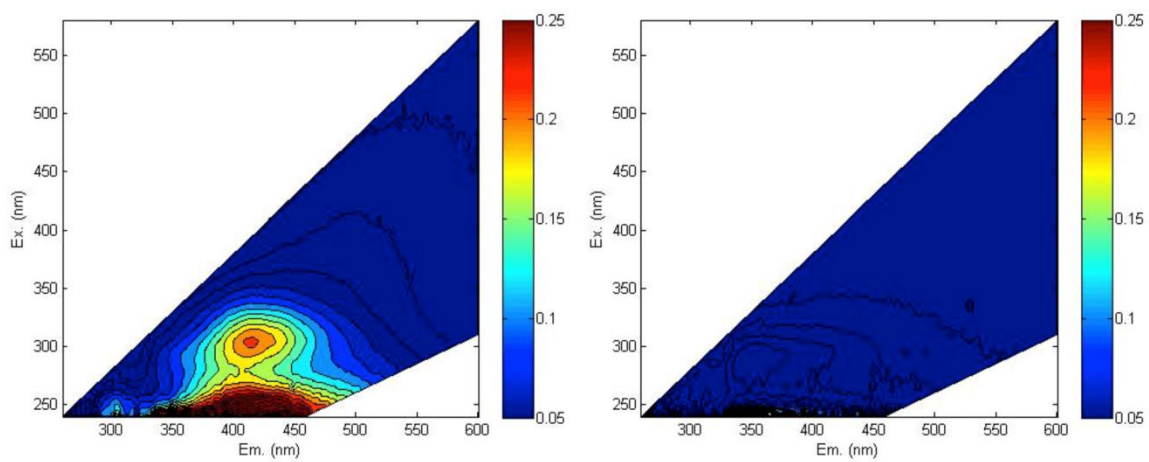


Figure 5.

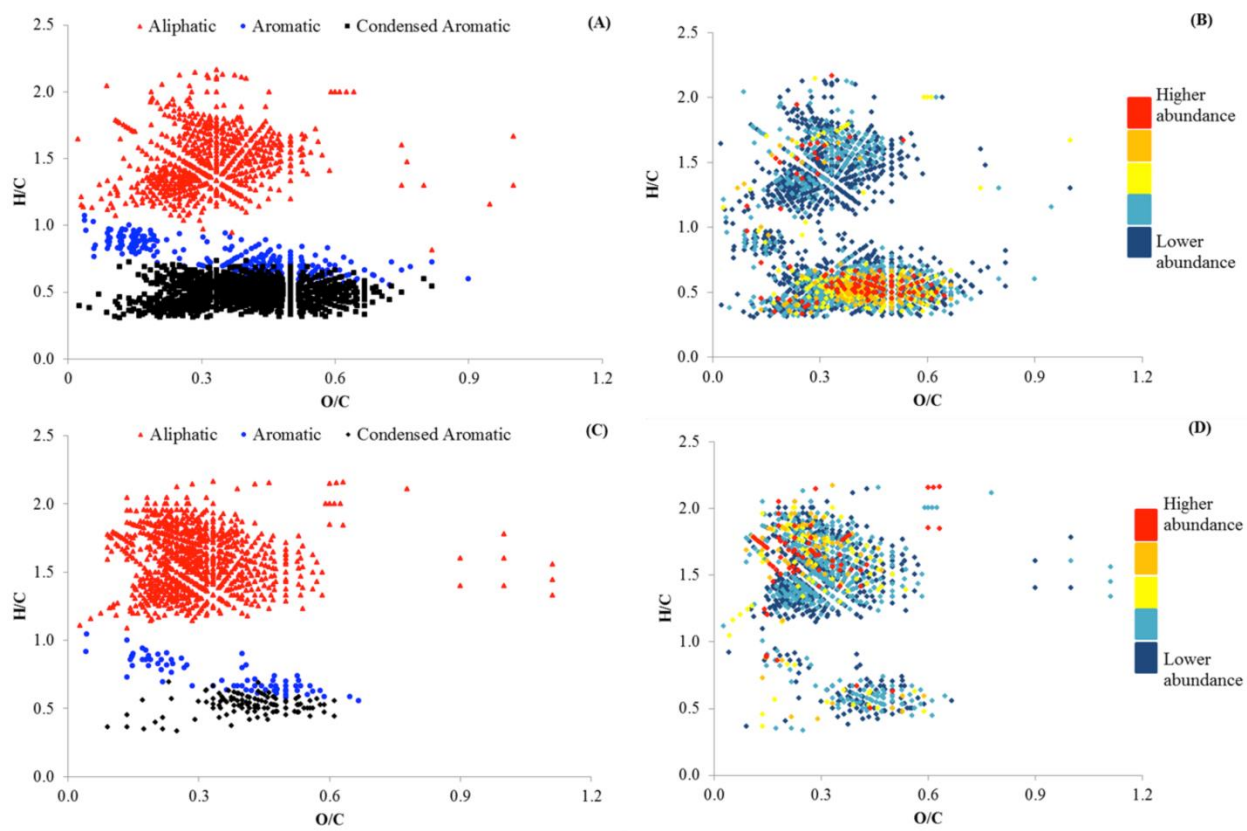
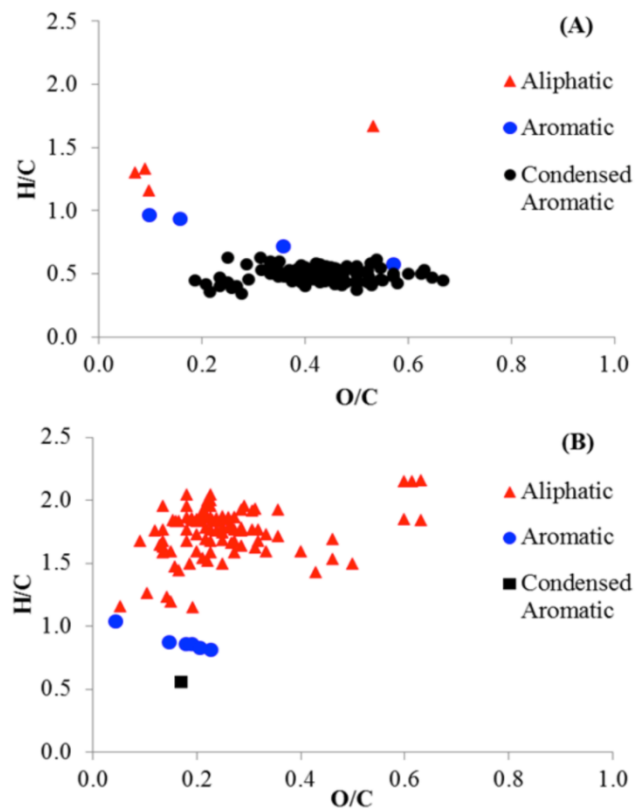


Figure 6.



Tables

Table 1. Elemental analysis of the precursor and charred biomass.

Biomass	% by mass				atomic ratios		
	C	H	N	O	ash	H/C	O/C
Precursor	49.81	6.02	0.78	34.91	8.54	1.45	0.53
	(0.18)	(0.04)	(0.02)	(0.19)	(2.15)	(<0.01)	(<0.01)
Charred	71.24	2.40	1.49	8.98	15.93	0.40	0.09
	(0.17)	(0.02)	(0.01)	(0.18)	(0.43)	(<0.01)	(<0.01)

Parentetical values are the standard deviation from the mean ($n = 2$ for all measurements, except for ash where $n = 6$).

Table 2. Summary of FT-ICR MS data for the dark control and light exposed dBC treatments.

dBC Treatment	# of Formulas	% of Formulas	% Spectral Magnitude	MW	H/C	O/C	DBE	AI _{mod}
Dark Control	2058	100%	100%	434 ± 86	0.88 ± 0.49	0.37 ± 0.14	14 ± 6	0.54 ± 0.30
Aliphatic	735	36%	33%	432 ± 82	1.49 ± 0.22	0.32 ± 0.11	7 ± 3	0.16 ± 0.15
Aromatic	235	11%	8%	430 ± 80	0.76 ± 0.11	0.37 ± 0.19	16 ± 3	0.59 ± 0.04
Condensed Aromatic	1088	53%	59%	435 ± 90	0.49 ± 0.09	0.40 ± 0.13	18 ± 4	0.77 ± 0.06
Light Exposed	1200	100%	100%	404 ± 75	1.42 ± 0.40	0.32 ± 0.13	7 ± 4	0.22 ± 0.23
Aliphatic	1016	85%	88%	406 ± 76	1.57 ± 0.21	0.31 ± 0.12	6 ± 3	0.14 ± 0.13
Aromatic	63	5%	5%	400 ± 67	0.77 ± 0.12	0.34 ± 0.16	15 ± 3	0.60 ± 0.05
Condensed Aromatic	121	10%	8%	388 ± 66	0.53 ± 0.07	0.42 ± 0.11	16 ± 3	0.73 ± 0.05

MW = molecular weight, DBE = double bond equivalents, and AI_{mod} = modified aromaticity index.

Values show ± standard deviation from the number averaged mean.

References

1. M. Moritz, M. Parisien, and E. Batllori, *Ecosphere*, 2012, **3**, 1–22.
2. P. E. Higuera, L. B. Brubaker, P. M. Anderson, T. A. Brown, A. T. Kennedy, and F. S. Hu, *PLoS One*, 2008, **3**, e0001744.
3. B. M. Jones, C. A. Kolden, R. Jandt, J. T. Abatzoglou, F. Urban, and C. D. Arp, *Arctic, Antarct. Alp. Res.*, 2009, **41**, 309–316.
4. M. C. Mack, M. S. Bret-Harte, T. N. Hollingsworth, R. R. Jandt, E. A. G. Schuur, G. R. Shaver, and D. L. Verbyla, *Nature*, 2011, **475**, 489–92.
5. L. Pessenda, S. Gouveia, and R. Aravena, *Radiocarbon*, 2001, **43**, 595–601.
6. J. Lehmann, J. Skjemstad, S. Sohi, J. Carter, M. Barson, P. Falloon, K. Coleman, P. Woodbury, and E. Krull, *Nat. Geosci.*, 2008, **1**, 832–835.
7. M. W. I. Schmidt, M. S. Torn, S. Abiven, T. Dittmar, G. Guggenberger, I. A. Janssens, M. Kleber, I. Kögel-Knabner, J. Lehmann, D. A. C. Manning, P. Nannipieri, D. P. Rasse, S. Weiner, and S. E. Trumbore, *Nature*, 2011, **478**, 49–56.
8. M. Elmquist, I. Semiletov, L. Guo, and Ö. Gustafsson, *Global Biogeochem. Cycles*, 2008, **22**.
9. E. A. Davidson and I. A. Janssens, *Nature*, 2006, **440**, 165–73.
10. M. C. Mack, E. A. G. Schuur, M. S. Bret-Harte, G. R. Shaver, and F. S. Chapin, *Nature*, 2004, **431**, 440–3.
11. E. A. G. Schuur, J. G. Vogel, K. G. Crummer, H. Lee, J. O. Sickman, and T. E. Osterkamp, *Nature*, 2009, **459**, 556–9.
12. C. A. Masiello, *Mar. Chem.*, 2004, **92**, 201–213.
13. M. Elmquist and G. Cornelissen, *Glob. Chang. Biol.*, 2006, **20**, 1–11.
14. X. Cao, J. Pignatello, Y. Li, C. Lattao, M. A. Campbell, N. Chen, M. F. Lesley, and J. Mao, *Energy & Fuels*, 2012, **26**, 5983–5991.
15. D. C. Podgorski, R. Hamdan, A. M. McKenna, L. Nyadong, R. P. Rodgers, A. G. Marshall, and W. T. Cooper, *Anal. Chem.*, 2012, **84**, 1281–1287.
16. S. Kim, L. A. Kaplan, R. Benner, and P. G. Hatcher, *Mar. Chem.*, 2004, **92**, 225–234.

17. W. C. Hockaday, A. M. Grannas, S. Kim, and P. G. Hatcher, *Org. Geochem.*, 2006, **37**, 501–510.
18. W. C. Hockaday, A. M. Grannas, S. Kim, and P. G. Hatcher, *Geochim. Cosmochim. Acta*, 2007, **71**, 3432–3445.
19. N. Singh, S. Abiven, M. S. Torn, and M. W. I. Schmidt, *Biogeosciences*, 2012, **9**, 2847–2857.
20. C. I. Czimczik and C. a. Masiello, *Global Biogeochem. Cycles*, 2007, **21**, 1–8.
21. R. Jaffé, Y. Ding, J. Niggemann, A. Vähätalo, A. Stubbins, R. G. M. Spencer, J. Campbell, and T. Dittmar, *Science*, 2013, **340**, 345–347.
22. T. Dittmar and B. P. Koch, *Mar. Chem.*, 2006, **102**, 208–217.
23. T. Dittmar, J. Paeng, T. M. Gihring, I. G. N. A. Suryaputra, and M. Huettel, *Limnol. Oceanogr.*, 2012, **57**, 1171–1181.
24. J. Major, J. Lehmann, M. Rondon, and C. Goodale, *Glob. Chang. Biol.*, 2010, **16**, 1366–1379.
25. S. Mitra, T. S. Bianchi, B. A. McKee, and M. Sutula, *Environ. Sci. Technol.*, 2002, **36**, 2296–302.
26. G. Guggenberger, A. Rodionov, O. Shibistova, M. Grabe, O. A. Kasansky, H. Fuchs, N. Mikheyeva, G. Zrazhevskaya, and H. Flessa, *Glob. Chang. Biol.*, 2008, **14**, 1367–1381.
27. M. L. Estapa and L. M. Mayer, *Mar. Chem.*, 2010, **122**, 138–147.
28. A. Stubbins, R. G. M. Spencer, H. Chen, P. G. Hatcher, K. Mopper, P. J. Hernes, V. L. Mwamba, A. M. Mangangu, J. N. Wabakanghanzi, and J. Six, *Limnol. Oceanogr.*, 2010, **55**, 1467–1477.
29. A. Stubbins, J. Niggemann, and T. Dittmar, *Biogeosciences*, 2012, **9**, 1661–1670.
30. L. A. Ziolkowski and E. R. M. Druffel, *Geophys. Res. Lett.*, 2010, **37**.
31. T. Dittmar, *Org. Geochem.*, 2008, **39**, 396–407.
32. R. M. Cory, K. McNeill, J. P. Cotner, A. Amado, J. M. Purcell, and A. G. Marshall, *Environ. Sci. Technol.*, 2010, **44**, 3683–9.
33. M. Gonsior, B. M. Peake, W. T. Cooper, D. Podgorski, J. D’Andrilli, and W. J. Cooper, *Environ. Sci. Technol.*, 2009, **43**, 698–703.

34. D. Kieber, J. McDaniel, and K. Mopper, *Nature*, 1989.
35. A. Mallakin, D. G. Dixon, and B. Greenberg, *Chemosphere*, 2000, **40**, 1435–1441.
36. B. McConkey and L. Hewitt, *Water. Air. Soil Pollut.*, 2002, **136**, 347–359.
37. K. Mopper and W. Stahovec, *Mar. Chem.*, 1986, **19**, 305–321.
38. K. Hammes, R. J. Smernik, J. O. Skjemstad, A. Herzog, U. F. Vogt, and M. W. I. Schmidt, *Org. Geochem.*, 2006, **37**, 1629–1633.
39. U. Hamer, B. Marschner, S. Brodowski, and W. Amelung, *Org. Geochem.*, 2004, **35**, 823–830.
40. G. Aiken, L. A. Kaplan, and J. Weishaar, *J. Environ. Monit.*, 2002, **4**, 70–74.
41. S. Tassan and G. M. Ferrari, *Appl. Opt.*, 2003, **42**, 4802–4810.
42. K. Spokas and D. Reicosky, *Ann. Environ. Sci.*, 2009, **3**, 179–193.
43. J. R. Helms, A. Stubbins, J. D. Ritchie, E. C. Minor, D. J. Kieber, and K. Mopper, *Limnol. Oceanogr.*, 2008, **53**, 955–969.
44. R. Cory, M. Miller, and D. McKnight, *Limnol. Oceanogr. Methods*, 2010, **8**, 67–78.
45. T. Dittmar, B. Koch, N. Hertkorn, and G. Kattner, *Limnol. Oceanogr. Methods*, 2008, **6**, 230–235.
46. R. L. Sleighter, G. A. McKee, Z. Liu, and P. G. Hatcher, *Limnol. Oceanogr. Methods*, 2008, **6**, 246–253.
47. F. W. McLaffert and F. Turecek, *Interpretation of Mass Spectra*, University Science Books, Sausalito, CA, 1993.
48. B. P. Koch and T. Dittmar, *Rapid Commun. Mass Spectrom.*, 2006, **20**, 926–932.
49. R. L. Sleighter, H. Chen, A. S. Wozniak, A. S. Willoughby, P. Caricasole, and P. G. Hatcher, *Anal. Chem.*, 2012, **84**, 9184–91.
50. S. Andrews, S. Caron, and O. Zafiriou, *Limnol. Oceanogr.*, 2000, **45**, 267–277.
51. Thomas W. Kirchstetter and T. Novakov, *J. Geophys. Res.*, 2004, **109**, D21208.
52. Y. Luo, M. Durenkamp, M. De Nobili, Q. Lin, and P. C. Brookes, *Soil Biol. Biochem.*, 2011, **43**, 2304–2314.

53. S. Abiven, P. Hengartner, M. P. W. Schneider, N. Singh, and M. W. I. Schmidt, *Soil Biol. Biochem.*, 2011, **43**, 1615–1617.
54. W. C. Hockaday, J. M. Purcell, A. G. Marshall, J. a. Baldock, and P. G. Hatcher, *Limnol. Oceanogr. Methods*, 2009, **7**, 81–95.
55. M. J. Norwood, P. Louchouart, L.-J. Kuo, and O. R. Harvey, *Org. Geochem.*, 2013, **56**, 111–119.
56. T. J. Battin, L. A. Kaplan, S. Findlay, C. S. Hopkinson, E. Marti, A. I. Packman, J. D. Newbold, and F. Sabater, *Nat. Geosci.*, 2008, **1**, 95–100.
57. B. T. Nguyen, J. Lehmann, W. C. Hockaday, S. Joseph, and C. A. Masiello, *Environ. Sci. Technol.*, 2010, **44**, 3324–31.
58. P. A. Raymond, J. W. McClelland, R. M. Holmes, A. V. Zhulidov, K. Mull, B. J. Peterson, R. G. Striegl, G. R. Aiken, and T. Y. Gurtovaya, *Global Biogeochem. Cycles*, 2007, **21**.